Medical Engineering and Physics 69 (2019) 17–27

Contents lists available at ScienceDirect

Medical Engineering and Physics

journal homepage: www.elsevier.com/locate/medengphy

Design and operation verification of an automated pressure mapping and modulating seat cushion for pressure ulcer prevention

Wei Carrigan[a], Pavan Nuthi[a], Charu Pande[a], Muthu B.J. Wijesundara[a,*], Cheng-Shiu Chung[b], Garrett G. Grindle[b], Joshua D. Brown[b], Benjamin Gebrosky[b], Rory A. Cooper[b]

[a] University of Texas at Arlington Research Institute, Fort Worth, TX, USA
[b] Human Engineering Research Laboratories, University of Pittsburgh, Pittsburgh, PA, USA

ARTICLE INFO

Article history:
Received 10 August 2018
Revised 22 March 2019
Accepted 6 June 2019

Keywords:
Seat cushion
Pressure ulcer prevention
Sensorized air cell
Real-time pressure mapping
Closed-loop control
Automated pressure modulation

ABSTRACT

A sensorized air cell-based seat cushion system was developed to address the issues of loading magnitude and duration at a sitting interface to aid in reducing risk of sitting acquired pressure ulcers. This system is capable of pressure mapping, redistribution, and offloading which were verified using an anthropomorphic model and a human subject. The system is comprised of an air cell array cushion, a pneumatic control unit, and a graphical user interface. ISO load deflection testing confirmed that the cushion's loading response is comparable to commercial air cell-based seat cushions. Testing demonstrated that the internal pressure of the air cells are indicative of interface pressure and can be used as input to pressure modulating algorithms. Uniform pressure distribution was achieved through automated pressure redistribution algorithm implementation where the immersion of a subject into the seat cushion increased and interface pressure decreased. High pressure point identification and automatic offloading were performed in which newly created high pressure points were addressed using subsequent redistribution. Pressure mapping enabled offloading and redistribution can objectively manage the effects of loading magnitude and duration at the sitting interface.

1. Introduction

Sitting acquired pressure ulcers (PU) are one of the main secondary medical complications experienced by individuals with physical and neurological conditions, such as spinal cord injury and stroke, who spend long periods of time in seated positions [1–3]. Though the etiology of PU formation is multi-factorial, mechanical compression and shear force acting upon skin, muscle, and fat against bony protuberances are postulated to be the main contributing factors [4,5]. Cells and tissues undergo deformation and ischemia when external mechanical loading exceeds physiological thresholds for magnitude and duration leading to PU formation [6]. As sitting concentrates approximately 50% of a person's bodyweight onto only 8% of their body's surface area, sitting may generate pressures in excess of 100 mmHg over vulnerable areas such as sacrum and ischial tuberosities, well above accepted pressure thresholds [7–10]. The degree of pressure on the body and the time required to begin PU formation are inversely proportional; therefore, this problem is exacerbated by longer sitting times as even lower seated pressure can lead to PU formation given a long enough time [11].

Current strategies attempt to mitigate PU formation by focusing on reducing the duration and magnitude of loading using frequent repositioning, offloading, and pressure reducing seat cushions. Clinical guidelines recommend that wheelchair users frequently perform pushups, rolling side-to-side, and forward-leaning to avoid pressure acting on the same region of the body over an extended period. Only individuals capable of independently performing these movements can adhere to these guidelines while those needing help must rely on caregivers [12–14]. However, the workload and availability of caregivers has become a barrier to providing adequate care [15–18]. To complement efforts at reducing PU formation, seat cushion technologies have been developed to relieve magnitude and duration of pressure.

Pressure reducing seat cushions employ two main strategies, namely passive and active pressure modulation [19]. Passive cushions employ foams, gel, air cell arrays, and customized surface geometries to reduce the magnitude of the peak interface pressure by increasing contact surface area through greater immersion of the person into the cushion [14,20]. Among them, air cell cushions have shown to provide higher immersion and can distribute

* Corresponding author.
E-mail address: muthuw@uta.edu (M.B.J. Wijesundara).

https://doi.org/10.1016/j.medengphy.2019.06.006
1350-4533/

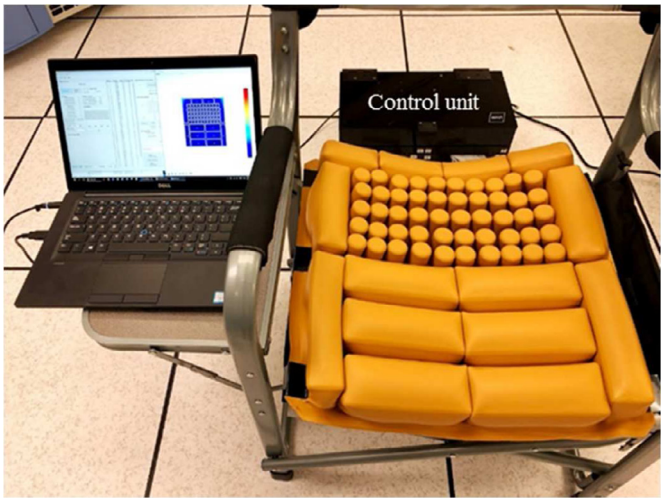

Fig. 1. The air cell array-based seat cushion with pneumatic control unit and GUI.

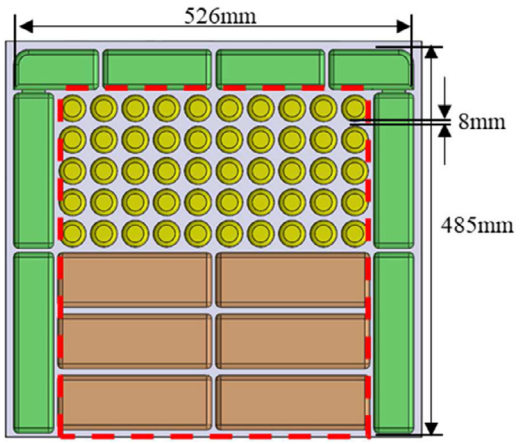

Fig. 2. Schematic of the 62 cell (two side cells at posterior corners are connected to each other and considered as a single cell) seat cushion layout and the overall dimension.

pressure more effectively than foam and gel cushions [21]. Customized contouring of foam seat cushions are also employed to fit the shape of a user's buttocks to maximize contact surface area. However, pathoanatomical changes of individuals over time can drastically alter the effectiveness of this approach [21]. Active seat cushions try to prevent long pressure durations by offloading certain areas at predetermined time intervals so as to relieve pressure and promote reperfusion [22–25]. A majority of the studied active seat cushions employ air cell arrays which are inflated and deflated to modulate pressures. Though effective at relieving the pressure in a given area, offloading in this manner can affect the surrounding areas whose tissues may experience significantly higher pressure and shear. An ideal active cushion should offload and address the consequences of offloading in a given area to reduce both the effects of magnitude and duration.

This paper presents a sensorized air cell array seat cushion system capable of relieving pressure and eliminating peak pressure points using real-time pressure mapping with closed-loop control. First, design considerations of the seat cushion, pneumatic control system, and graphical user interface (GUI) are briefly discussed. Secondly, the system's real-time pressure mapping capability is verified with a commercial pressure sensing mat. This examines the system's ability to accurately detect the pressure profile of a seated person which is used as the control input for modulating air cell pressure. Finally, the pressure redistribution and offloading capabilities are demonstrated with an anthropomorphic model and a seated individual.

2. System description

The system (Fig. 1) consists of an air cell array-based seat cushion, a controller with electronic and pneumatic components, and a GUI [26]. Each cell in the cushion acts as both a sensor and an actuator where the internal pressure of the cells are used for detecting and modulating interface pressure. The internal pressure of each cell is individually controlled using a corresponding pressure sensor and a valve. The GUI provides commands to the controller for pressure modulating algorithm while it records and displays the internal pressure profile of the seat cushion. This continuous pressure mapping capability enables accounting for both the duration and magnitude of pressures acting on the sitting interface regardless of individuals' posture, size, shape, and weight. Pressure mapping coupled with control algorithms allows for the automatic identification and modulation of interface pressure through offloading and redistribution.

3. Seat cushion design and fabrication

This seat cushion uses a combination of different sized air cells in arrays which are designed to modulate the pressure across a sitting surface. The cushion (Fig. 2) consists of active and passive regions where the active region participates in pressure modulation and the passive region, shown outside of the dashed line, provides stability. These passive cells are inflated to a constant pressure and are not used in modulation operations. The cells within the active region are of two designs: smaller cells for the posterior and larger rectangular cells for the anterior. The arrangement of the posterior and anterior cells are of 5×10 and 3×2 arrays, respectively, with a space of 8 mm in-between. Clinical observations have shown that pressure concentrations occur primarily in the posterior region of the buttocks. These high pressure points are often located on and around the bony prominences i.e., ischial tuberosities (IT) and the coccyx [27,28]. Air cells in the posterior of the cushion enable identification and modulation of pressure under these bony prominences. The design of the posterior cells are cylindrical with a diameter of 33 mm which was selected to provide a unit area of 854.87 mm^2, significantly smaller than the reported contact area of 3349.1 mm^2 under IT [29,30]. Anterior region cells have a unit area of 185 mm $\times$ 70 mm which was chosen based on the absence of bony prominences within this region of the body. Furthermore, the larger cells were primarily created for load bearing and simplifies the control aspect by reducing the number of cells. All cells have a height of 70 mm that allows for an immersion greater than the distance between the IT and great trochanter, which is about 50 mm [31]. The extra 20 mm prevents the seat cushion from bottoming out during sitting and allows for deflation if needed during pressure modulation. This distance was also within the suggested range of 12.7 mm to 25.4 mm, which is the distance from the IT to a wheelchair seat after immersion within air cell-based seat cushions [29,32].

The seat cushion was manufactured using a standard dip molding process combined with a bonding process which is commonly employed for air cell-based seat cushion manufacturing. The dip molding process consisted of sequential dipping of neoprene, latex, and neoprene rubber that produce cells with multilayer elastomers. The inner and the outer neoprene layers have approximate thicknesses of 0.37 mm and 0.21 mm while the middle latex layer has a thickness of 0.42 mm. Enclosing latex in-between the neoprene rubber layers ensures no latex is in contact with the user. The overall cushion size is 526 mm $\times$ 485 mm $\times$ 70 mm ($W \times D \times H$) which matches the dimensions of a large size commercial cushion.

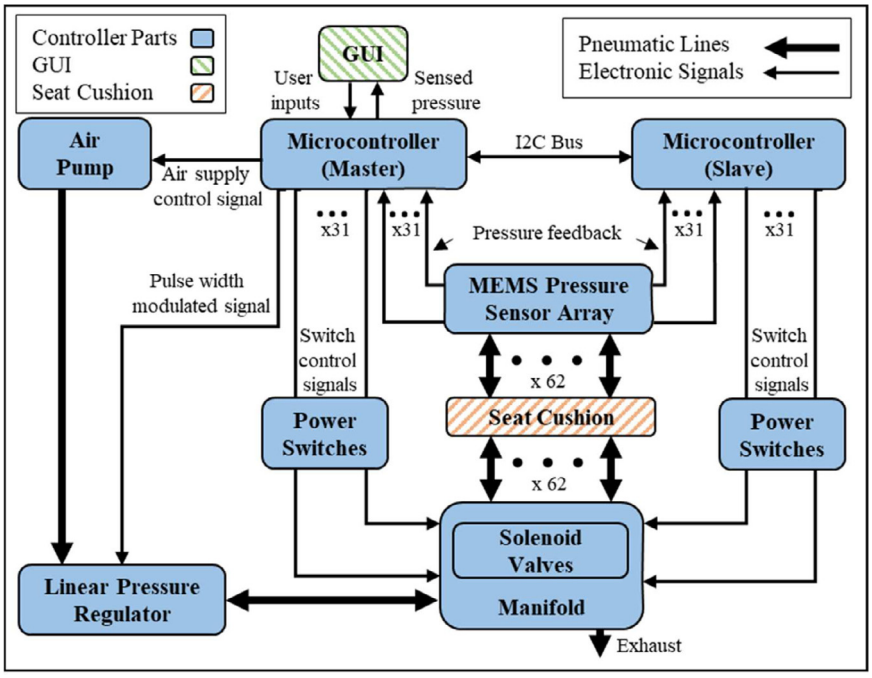

Fig. 3. Pneumatic and electronic layout of the seat cushion and control hardware showing each microcontroller managing half (31 air cells) of the seat cushion.

4. Pneumatic control unit

The control unit was a collection of pneumatic and electronic components designed to achieve a closed-loop control for internal pressures of 62 air cells. These components included two microcontrollers in a Master-Slave configuration which communicated through an I2C bus, an array of solenoid valves with the same number of electrically controlled power switches and air pressure sensors, a miniature air pump, and a pressure regulator (Fig. 3). The solenoid valve arrays were grouped into 4 sets of 16 and were connected to a common manifold. These air lines supplied 62 air cells through a common manifold while providing two additional lines for exhaust of the manifold. Similar to the solenoid valves, internal air pressure sensors were connected to each air cell which report to their corresponding microcontroller. Additionally, the air pump was connected to the common manifold via the pressure regulator which supplies air at a reduced pressure with a consistent flow rate.

To address the high number of inputs and outputs, a two microcontroller solution was chosen. Half of the air cells were monitored and controlled by the Master microcontroller with the rest addressed by the Slave. Since common resources such as the air pump and pressure regulator can only be controlled by one microcontroller, all the inputs and outputs addressed by the Slave microcontroller were transmitted to the Master to inform its control implementation. Hence, the only job of the Slave microcontroller was to relay messages between the Master and the connected pneumatic hardware. The control algorithm implemented on the Master microcontroller ensures that the commanded pressure profile from the GUI was achieved in all air cells using the pneumatic hardware of the control unit.

The control objective was to regulate the internal pressures P_{sens_i} so that $|P_{sens_i} - P_{com_i}| < \sigma$ for a small enough σ value, where P_{sens_i} is the sensed internal pressure and P_{com_i} is commanded pressure of the i^{th} air cell. The σ value was chosen to be 0.35 kPa based on a pressure sensor resolution of 0.05 kPa and response time of the controller hardware through system characterization. The solenoids s_i connect the cells to the common manifold and the exhaust solenoid s_e connects the common manifold to the atmosphere. The air cell solenoids s_i, exhaust solenoid s_e, and linear pressure regulator P_{lpr} are considered control inputs, whereas P_{sens_i} are considered outputs to be regulated. Given the pneumatic layout of the seat cushion system, a novel scheduling bang-bang controller was implemented along with time division multiplexing to share the common resources of air pump and regulator for achieving simultaneous regulation of internal pressure in all cells [26,33].

A custom GUI (Fig. 4) was developed to capture pressure data, display a pressure profile, and accept user input. A majority of the space in the GUI was used to display the internal pressure data in various representations. The pressure sensor data was used to create an interpolated pressure profile which was then displayed as a live three dimensional surface map. Additionally, the GUI also displayed raw internal pressure data from each sensor as well as average pressure of various areas (e.g. thigh, buttock, left, right) for convenience of the user. The raw pressure data can be collected and saved to a given file name along with a time stamp using two modes: (i) a snapshot of pressures captured at any moment and (ii) a recording of pressures captured for a specified length of time. A pressure control panel along with a manual area selection panel can be used to command the internal pressure of any air cell or a group of air cells. The pressure control panel also enables control for more automated pressure modulation operation including pressure offloading and redistribution. This GUI was developed in Python environment using the 'pygtk' library which performs all of the above functions without the use of any proprietary software or hardware.

5. Load-bearing and hysteresis tests

Tests were conducted with standard wheelchair seat cushion test setup to verify the load-bearing capability and the corresponding immersion of the manufactured seat cushion following the guidelines of ISO 16840-2 [34]. Setup included a Rigid Cushion Loading Indenter (RCLI) attached to a Material Testing System (MTS 58 Bionix II) that allows for uniaxial loading in the vertical direction of the cushion up to 750 N and measuring the travel distance of the RCLI, which will account for the immersion of the cushion

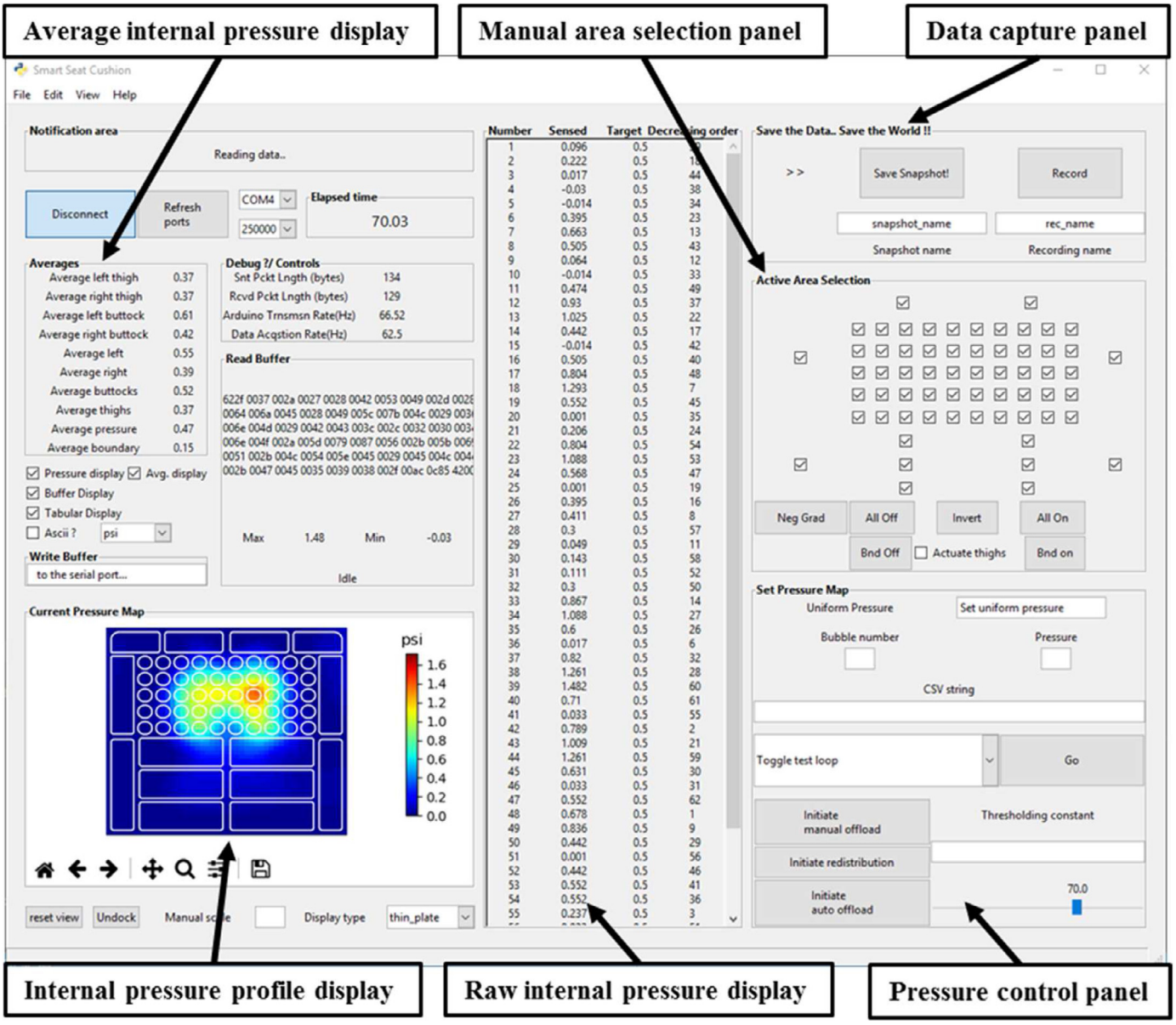

Fig. 4. Python-based GUI for the operation and monitoring of the seat cushion.

during loading and unloading. As shown in Figure 5, the seat cushion was placed on the base plate of the MTS and was aligned with the RCLI so that the IT of the indenter were supported by the small cylindrical air cells while the thigh area was supported by the large rectangular air cells.

To examine the cushion behavior at different initial inflation pressures, three different inflation cases were used in the active region while the bordering passive air cells were kept at constant pressure of 2.8 kPa. All active air cells were inflated uniformly to gauge pressures of 0 kPa, 1.4 kPa, and 2.8 kPa that were similar in magnitude to values suggested for air cell-based seat cushions where higher inflation pressure indicates higher stiffness [28]. Each test was conducted three times to ensure repeatability. The internal pressure of all air cells in the cushion and displacement of the RCLI during the loading and unloading phases were recorded both to continuously examine the integrity of the cushion when subject to high loads and to calculate the hysteresis from load-deflection curves.

Figure 6(a) shows the time trajectories of sensed and commanded axial force during the load-deflection test where the

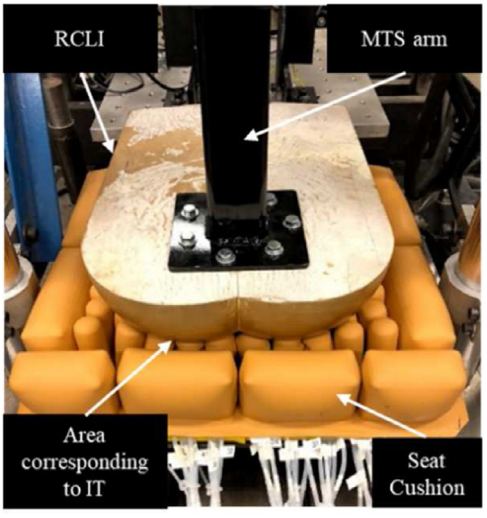

Fig. 5. Standard wheelchair seat cushion test setup.

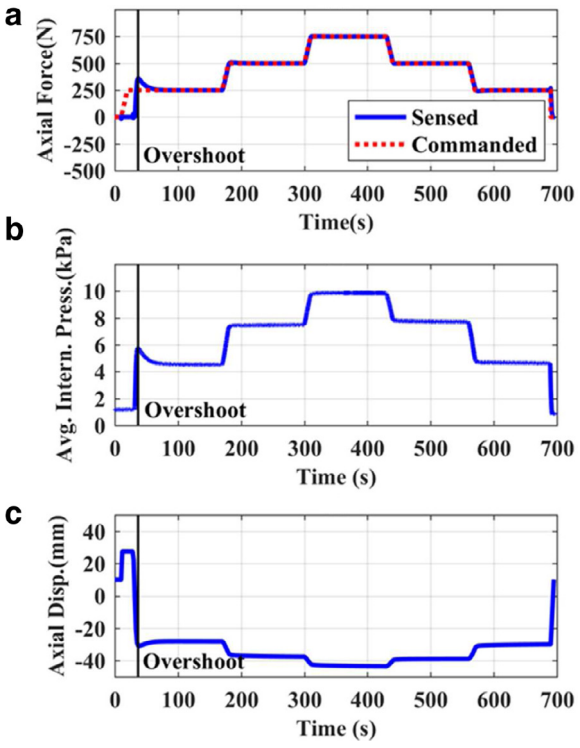

Fig. 6. Time trajectories of (a) sensed and commanded axial forces, (b) average internal pressure among all air cells, (c) recorded axial displacement during the load deflection test conducted with initial inflation pressure of 1.4 kPa.

initial inflation pressure was set to 1.4 kPa. The cushion was subjected to step-wise compression and unloading with applied forces of 250 N, 500 N, and 750 N for set time intervals and ramping rates. The force trajectories indicate that the MTS maintained the commanded axial force on the seat cushion with acceptable overshooting behavior most noticeable at time = 37 s during the initial ramp up to 250 N, also occurring to an infinitesimal degree at every other force increment. The trajectory of the average internal pressure of the active air cells, shown in Figure 6(b), shows instant change when the loading conditions vary indicating a spontaneous reaction of the air cells when responding to changes in external loads. This characteristic allows the cushion to capture real-time internal pressure changes to assist with pressure modulation. The recorded axial displacement, Figure 6(c), of the MTS was the travel distance of the RCLI and shows the compression of the cushion. Continuously recorded displacement was plotted against time where negative values indicate that the MTS was moving downwards and zero displacement indicates the position where the RCLI made contact with the cushion with no significant force applied. Note, there was upward movement of the RCLI before ramping the force to 250 N that was due to the inherent characteristic of MTS system where the MTS pulled up and then moved down to compress the cushion. Similarly, after the completion of the test, the RCLI retracted back about 10 mm above the cushion. As expected, the displacement increased during the compressing phase and reached maximum displacement of 43.25 mm at the load of 750 N, which ensured the cushion's immersion capability and load capacity while preventing the cushion from "bottoming-out".

Table 1
Hysteresis indices at 250 N, and 500 N loading conditions for various initial inflation conditions.

Inflation pressure (kPa)	Hysteresis index at 250N	Hysteresis index at 500N
0	0.040	0.027
1.4	0.039	0.032
2.8	0.032	0.038

The same tests were performed with initial inflation pressures of 0 kPa and 2.8 kPa and force-displacement plots of all three cases are shown in Figure 7. Lower pressure provides more immersion showing the cushion was more compliant while, conversely, higher pressure shows less immersion resulting from higher resistance implying a stiffer cushion. These findings align with the conclusions obtained from ISO tests of other commercial seat cushions where the trend of the gradient denotes the stiffness of the cushion which indicates its ability to envelop around the pelvis. A shallower gradient indicates a stiffer cushion and a compliant cushion usually has a steeper curve [35].

The hysteresis index, also known as the resilience, indicates the energy dissipation capability as well as the tendency of the seat cushion to come back to its original shape. A higher resilience indicates greater dissipation and damping of the mechanical energy transferred through the seat cushion; however, it also indicates a slow rate of recovery in returning to its original shape after a load was removed. Thus, there exists a prescribed range for appropriate resilience between 0.02–0.3 which is within the range of commercial wheelchair seat cushions [34]. The hysteresis was calculated using the formula provided in the ISO guideline with the input of the cushion thickness at two loading steps including compressing and unloading, as seen in Eq. (1) [35]. The calculated hysteresis for three inflation cases is listed in Table 1 which indicate that our seat cushion was in the lower end of the prescribed range that corresponds to low energy dissipation and fast response to load changes. The hysteresis indices for the seat cushion were the closest to the commercially available air cell-based cushion (ROHO Single valve cushion) which evaluates at 0.096 for 250 N, and 0.043 for 500 N [34]. The indices indicate that the seat cushion was faster

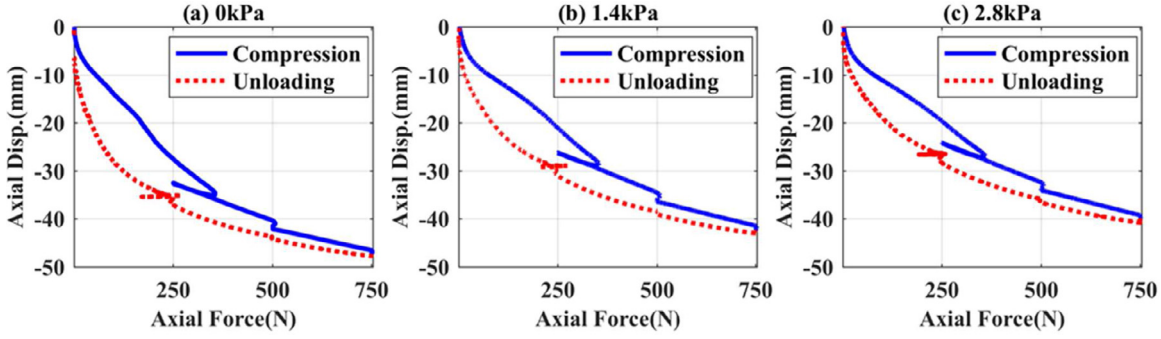

Fig. 7. Phase plot of measured axial displacement vs. applied axial force during both compression and unloading phases of the load-deflection tests at various initial inflation pressures of the seat cushion: (a) 0 kPa, (b) 1.4 kPa, and (c) 2.8 kPa.

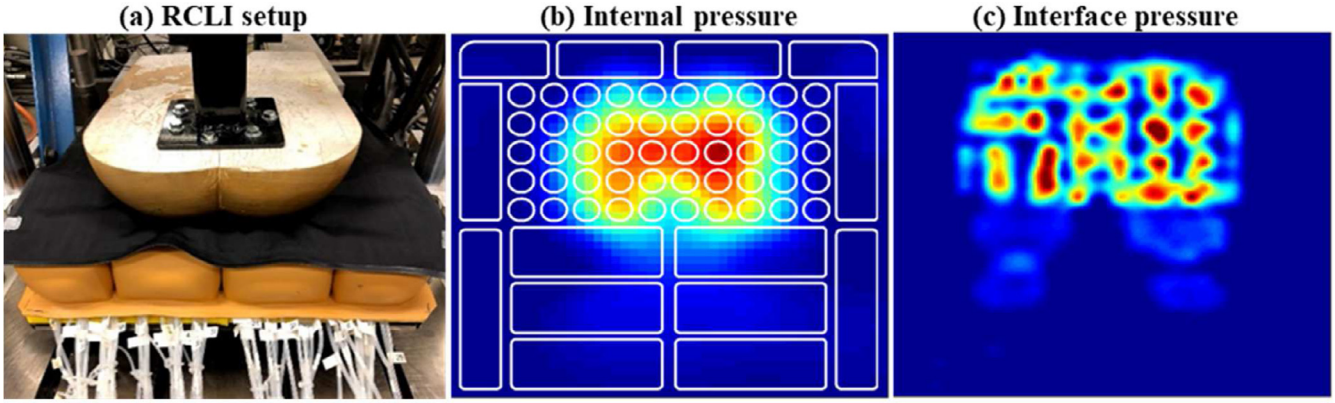

Fig. 8. (a) Test setup used for conducting pressure mapping, (b) internal pressure profile when 500 N is applied on a cushion with 0 kPa inflation pressure, and (c) corresponding interface pressure profile.

than the ROHO cushion when it responds to changes in loading conditions. This will allow the seat cushion to perform pressure sensing and pressure modulation with minimal lag and at a relatively higher frequency.

$$\textit{Hysteresis index at } 250N = 1 - \frac{\overline{h_{250u}}}{\overline{h_{250c}}}$$

$$\textit{Hysteresis index at } 500N = 1 - \frac{\overline{h_{500u}}}{\overline{h_{500c}}} \quad (1)$$

6. Pressure modulation test

6.1. Interface and internal pressure mapping

The internal pressure and interface pressure profiles should match in regards to pressure distribution in order to use the internal pressure of the air cells for modulation of the interface pressure. Testing of the pressure mapping of the seat cushion was verified using a commercial interface pressure sensor mat (BT1526, BodiTrak) that was placed on the cushion after inflation to 0 kPa, shown in Figure 8(a). A static load of 250 N, 500 N, and 750 N was applied using the MTS to mimic body weights of 51 kg, 102 kg, and 153 kg assuming 50% of the body weight is supported by the cushion [7]. Internal pressure maps shown are extrapolated over a uniform grid using 'biharmonic spline' method while the interface pressure maps are extrapolated by the BodiTrak software. The internal pressure and interface pressure data were recorded simultaneously and representative pressure maps for the 500 N case are shown in Figure 8(b) and (c) with similar results observed for 250 N and 750 N. The magnitude and profile of both interface and internal pressures showed similar trends with the posterior section of the buttock model having deeper immersion than the anterior resulting in concentrated pressure in the posterior. This shows a consistent agreement reflected among all the loading scenarios and confirms that the internal pressure of air cells can be used as a representation for the interface pressure.

Additionally, testing was performed with a human subject who changed their sitting posture to verify the system's ability to recognize posture and high pressure points in a real world scenario. The pressure profiles for different sitting postures (sitting upright, leaning left, and leaning right) are displayed in Figure 9(a)–(c). These data confirm consistent agreement between the internal and interface pressure profiles at each posture and the ability of the seat cushion to identify postural changes with a distinct pressure profile corresponding to anatomical features in a human subject [36].

6.2. Redistribution test

To investigate the cushion's pressure redistribution capability, a redistribution test was performed where the algorithm equalizes the air pressure in all air cells. Multiple redistribution phases are used to obtain lowest possible internal pressure without bottoming out. In phase 1, the common inflation pressure is determined by the calculated average of internal pressures of all air cells. In subsequent phases the common inflation pressure is reduced by equal decrements. The seat cushion was pre-pressurized to 1.4 kPa and a static load of 500 N was maintained. The interface and internal pressure profile at each phase are plotted before loading in Figure 10(a) and after loading in Figure 10(b). The average pressure among all active air cells upon loading was calculated to be 7.3 kPa which was used as the common pressure among all active cells in the first pressure redistribution. As seen in Figure 10(c), the concentrated pressure in the posterior was reduced and the interface pressure became more evenly distributed. The contact surface area increase in the interface profile implies that immersion has increased. Further reduction of redistribution pressure in subsequent phases shows more uniformly distributed interface pressure with increased contact area, shown in Figure 10(d)–(f).

Results showed that the maximum and average values of the interface pressure were reduced as the redistribution phases progressed, seen in Figure 11(a), with a significant maximum reduction at the first redistribution phase. Since all active air cells were pressurized equally to a specific value which was reduced throughout the phases, the maximum pressure and the calculated average pressure were not significantly different. From comparing Figures 10 and 11(a), it can be determined that the interface pressure profile was not uniform across the cushion surface as there were localized pressure concentrations, possibly attributed to the sharp deformation of the interface pressure mat due to the non-continuous nature of the seat cushion surface. These pressures were always outliers compared to the average where magnitudes remain around 17 kPa despite shifts in location after each pressure redistribution.

During the pressure redistribution test, the displacement of the RCLI was recorded as a measure of immersion. As shown in Figure 11(b), a significant immersion occurred as the load was applied, with further immersion occurring as pressure redistribution phases progressed. This factor determines when the redistribution terminates as the remaining height of an air cell under load must maintain approximately 25 mm to avoid bottoming out. In this case, the final redistribution pressure was 3.16 kPa with an immersion exceeding 50 mm. This pressure was considered optimal for air cell-based cushions [28]. This pressure redistribution technique

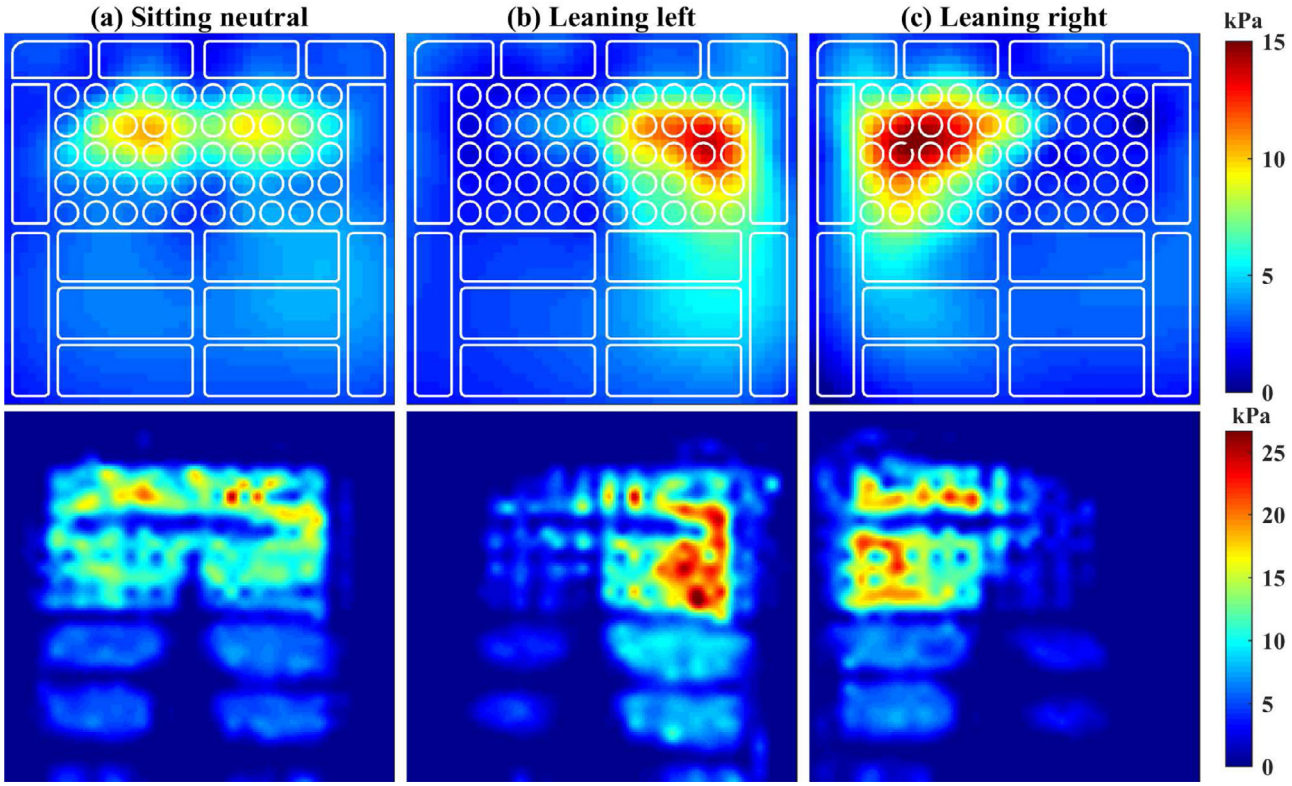

Fig. 9. Internal (top) and interface (bottom) pressure profiles with various sitting postures (a) sitting upright, (b) leaning left, and (c) leaning right.

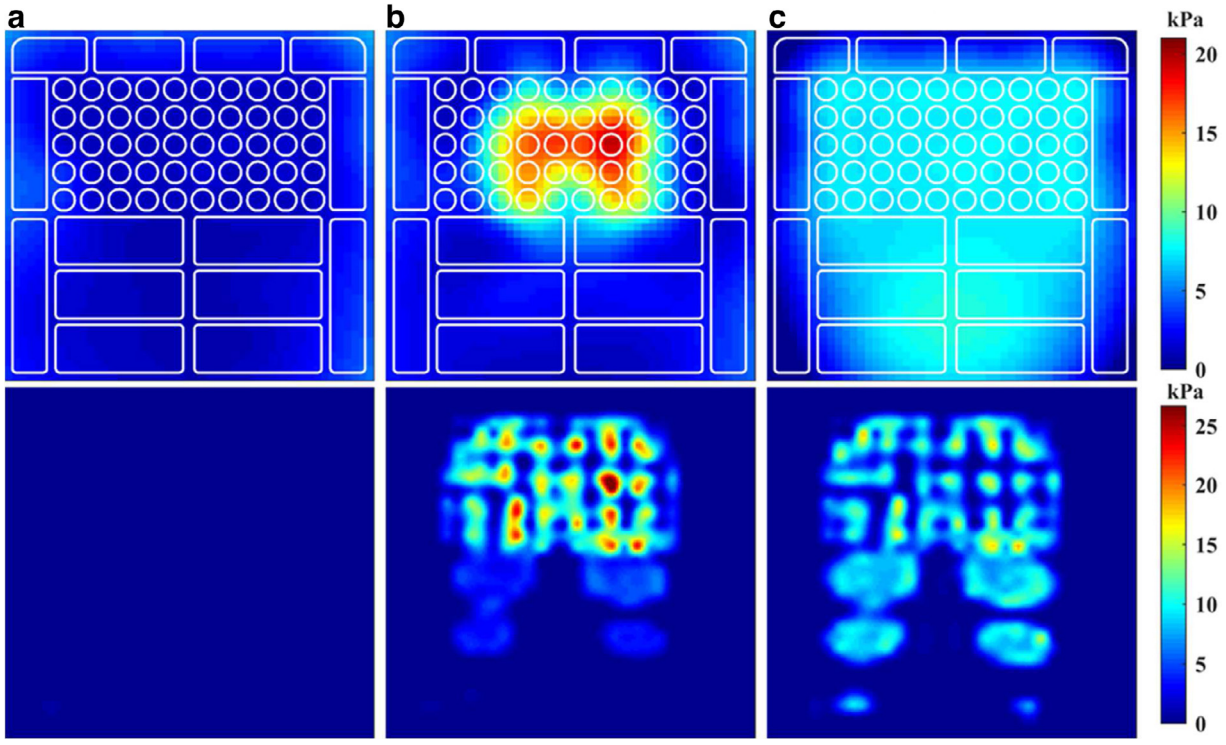

Fig. 10. Part I: Internal (top row) and interface (bottom row) pressure profile generated at each pressure modulation phase (a) after pre-pressurizing seat cushion to 1.4 kPa, (b) when applying a static load of 500 N, and (c) after assigning a pressure of 7.3 kPa to all air cells (redistribution phase 1).
Part II: Internal (top row) and interface (bottom row) pressure profile generated at each pressure modulation phase (d) further reducing the redistribution pressure to 5.92 kPa (phase 2), (e) at redistribution pressure of 4.54 kPa (phase 3), and (f) final redistribution pressure of 3.16 kPa (phase 4).

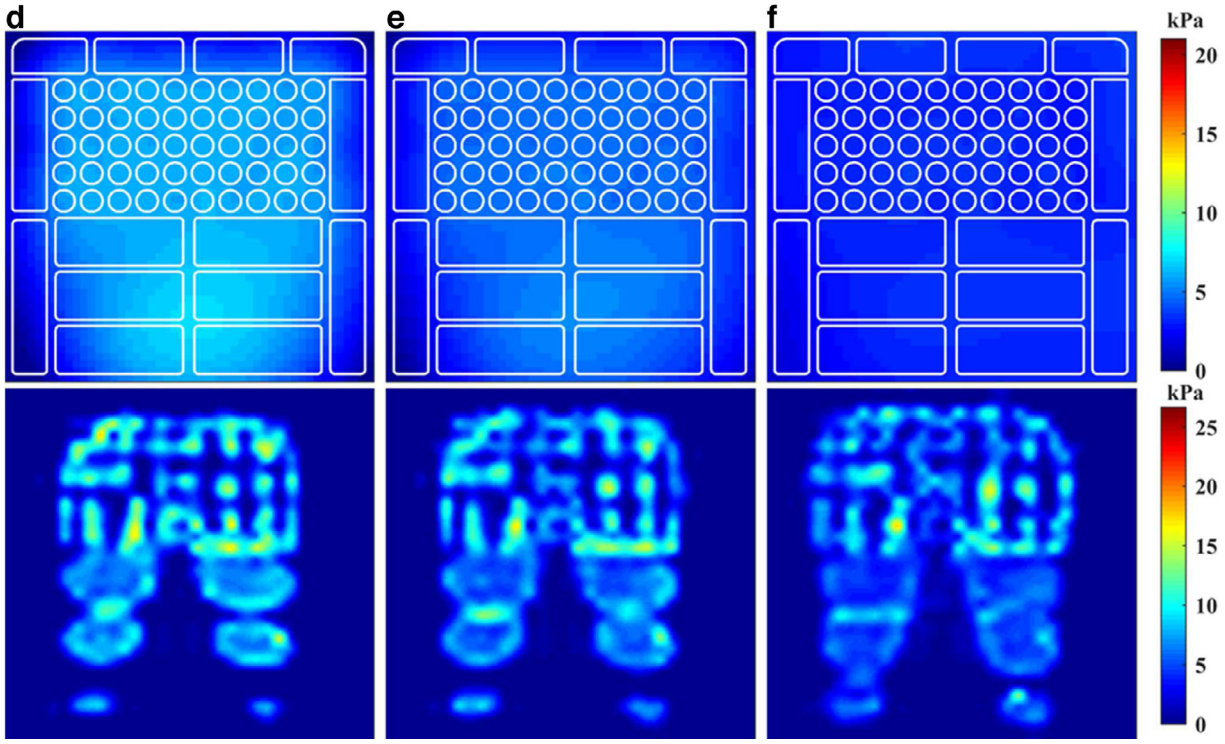

Fig. 10. Continued

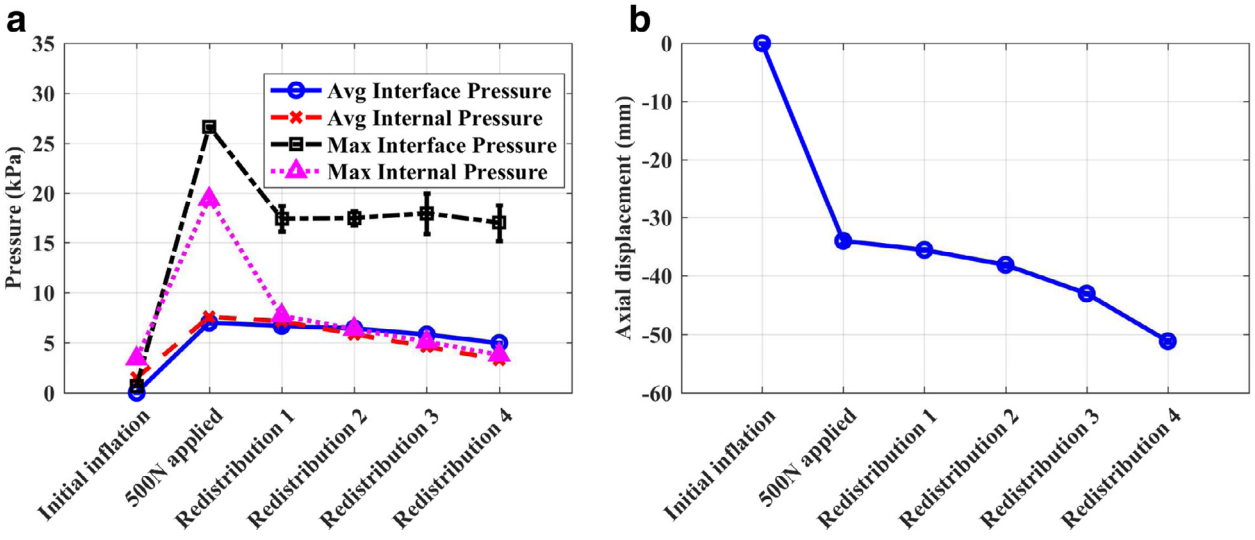

Fig. 11. (a) Maximum and average pressure of internal and interface pressure and (b) recorded displacements at each redistribution phase.

was not only capable of providing a more uniform pressure distribution conforming to the pelvis, but increases the immersion, both of which are considered key factors in pressure ulcer prevention strategies [14,20,21].

Similar to pressure mapping tests, redistribution testing was performed with a seated human subject in a natural upright position where the cushion was pre-pressurized to 1.4 kPa. Upon sitting, the average pressure in the air cells rose to 5.17 kPa and a three-phase pressure redistribution was carried out until the final pressure was reduced to 2.37 kPa, seen in Figure 12(a)–(d). Captured pressure profiles indicate that pressure uniformity as well as the contact surface area increased with each redistribution step.

6.3. Pressure offloading test

After confirming pressure redistribution capability, the pressure offloading test was conducted to verify the automated peak pressure identification and offloading capability of the cushion. The same test setup was used as in the previous test with the exception of the pressure mat as it would interfere with offloading. The seat cushion was pre-pressurized to 1.4 kPa, shown in Figure 13(a), and then compressed with the RCLI at 500 N as seen in Figure 13(b). An automated pressure relief algorithm was executed to remove high pressure points above a calculated threshold value based on the sensed pressure profile, seen in Figure 13(c). The threshold pressure value is a percentage of the linear sum of

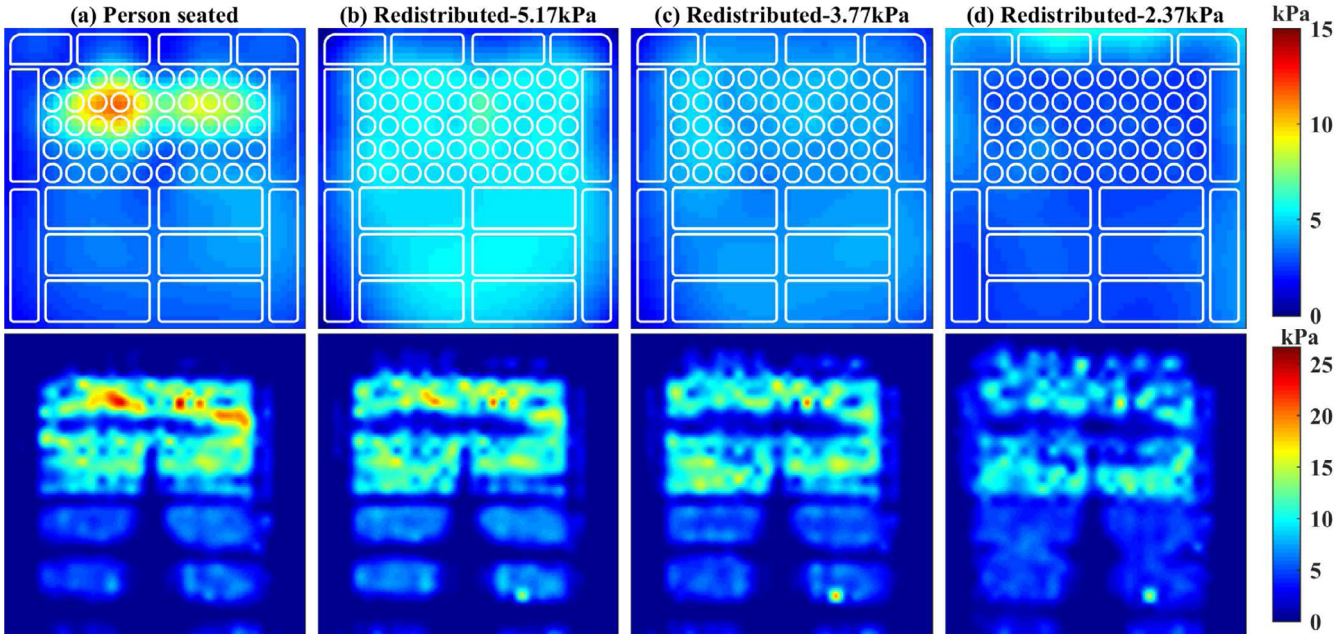

Fig. 12. Internal (top) and interface (bottom) pressure profiles through various phases of redistribution (a) upright posture before redistribution, (b) all air cells redistributed to 5.17 kPa, (c) redistributed to 3.77 kPa, and (d) redistributed to 2.37 kPa.

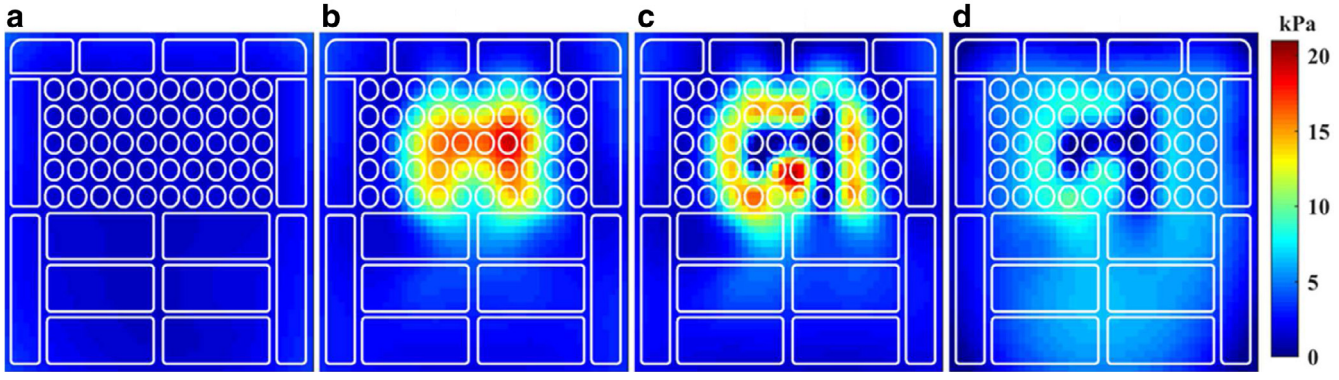

Fig. 13. Internal pressure profiles for various stages of offloading and redistribution (a) initial inflation to 1.4 kPa, (b) compression at 500 N, (c) offloaded high pressure areas determined by 30% thresholding parameter, and (d) redistributed pressure in remaining air cells.

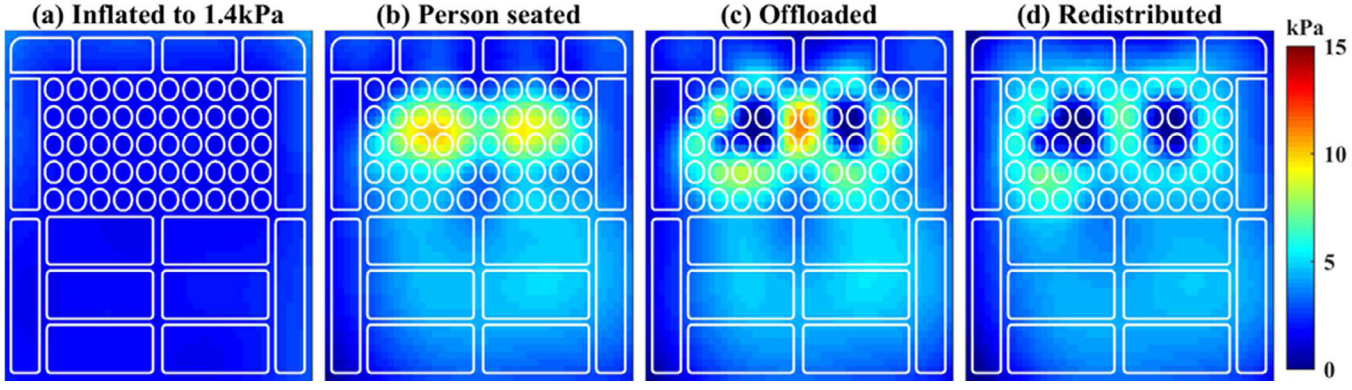

Fig. 14. Internal pressure profiles through various stages of offloading and redistribution (a) initial inflation of 1.4 kPa, (b) person seated at an upright position, (c) offloaded high pressure areas determined by 30% thresholding parameter, and (d) redistributed pressure in remaining air cells.

minimum and maximum internal pressure values which can be adjusted based on the need of the patient where a higher threshold value results in less offloaded air cells. Offloading results in a new pressure profile with newly created high pressure points in areas surrounding and supporting the offloaded air cells. Subsequent pressure redistribution was implemented to remove these new high pressure points and uniformly distribute the load among the remaining air cells without interfering with the offloaded cells as seen in Figure 13(d). For accommodating medical conditions, such as deformity and pre-existing wounds, the pressure can be manually removed at known locations to avoid loading in sensitive areas and will not affect the pressure redistribution procedure.

The automated pressure offloading-redistribution capability was also verified with a seated person and the internal pressure profiles were plotted in Figure 14(a) and (b). The concentrated pressures under the IT areas were successfully removed with the same threshold value used in the RCLI test (as seen in Figure 14(c)) and the resulting high pressure points were further reduced by a subsequent redistribution, seen in Figure 14(d).

7. Conclusions

We have successfully demonstrated the pressure management capability and characteristics of a sensorized air cell-based seat cushion including load response, real-time pressure mapping, redistribution, and adaptive pressure offloading. The cushion was verified with an ISO load deflection test for hysteresis and is comparable to commercial air cell-based seat cushion behavior. This testing also confirmed the real-time pressure mapping capability of the system in response to dynamic loading changes. Further, we have confirmed that sensed internal air pressure can be used as an analog for the interface pressure. Therefore, it was concluded that this internal pressure can be used as an input for pressure redistribution and offloading algorithms.

We observed that as pressure redistribution phases progressed, immersion was increased while the contact pressure was reduced and uniformly distributed. Furthermore, this system was able to identify and automatically redistribute newly created high pressure points after offloading. This confirms that our seat cushion technology is capable of addressing the issues of loading magnitude at the sitting interface. As the algorithm can react to the dynamic changes of a user's seated posture, it could therefore be used to manage the duration of loading at this interface.

Advantage of this technology over other seat cushions is that it will reduce the caregiver's and user's intervention in the current practice of time based repositioning. Sensor driven modulation enables objective pressure relief strategies. However, the dimensions of the prototype as well the size of control hardware make the integration possible for a limited section of wheelchairs. In future works, we plan to reduce the form-factor of the control unit and examine the seat cushion behavior such as dynamic stability, usability, and safety.

Conflict of interest statement for the manuscript

No conflict of interest to report.

Competing interests

None declared.

Funding

This works was supported by the Office of the Assistant Secretary of Defense for Health Affairs through the Spinal Cord Injury Research Program under Award no. W81XWH-15-1-0719. Opinions, interpretations, conclusions and recommendations are those of the author and are not necessarily endorsed by the Department of Defense.

Ethical approval

Not required.

References

[1] Fard FD, Moghimi S, Lotfi R. Evaluating pressure ulcer development in wheelchair-bound population using sitting posture identification. Engineering 2013;5:132–6. http://dx.doi.org/10.4236/eng.2013.510B027.
[2] Geyer MJ, Brienza DM, Karg P, Trefler E, Kelsey S. A randomized control trial to evaluate pressure-reducing seat cushions for elderly wheelchair users. Adv Skin Wound Care 2001;14(3):120–9.
[3] Zacharkow D. Wheelchair posture and pressure sores. IL: Springfield; 1984.
[4] Loerakker S, Stekelenburg A, Strijkers GJ, Rijpkema JJ, Baaijens FP, Bader DL, Nicolay K, Oomens CW. Temporal effects of mechanical loading on deformation-induced damage in skeletal muscle tissue. Ann Biomed Eng 2010;38(8):2577–87.
[5] Hoogendoorn I, Reenalda J, Koopman BFJM, Rietman JS. The effect of pressure and shear on tissue viability of human skin in relation to the development of pressure ulcers: a systematic review. J Tissue Viability 2017;26(3):157–71.
[6] Moore Z, van Etten M. Repositioning and pressure ulcer prevention in the seated individual. Wounds UK 2011;7(3):34–40.
[7] Staas WE, Cioschi HM. Pressure sores—a multifaceted approach to prevention and treatment. Western J Med 1991;154(5):539–44.
[8] Brienza DM, Karg PE, Geyer MJ, Kelsey S, Trefler E. The relationship between pressure ulcer incidence and buttock-seat cushion interface pressure in at-risk elderly wheelchair users. Arch Phys Med Rehabil 2001;82(4):529–33.
[9] Makhsous M, Rowles DM, Rymer WZ, Bankard J, Nam EK, Chen D, Lin F. Periodically relieving ischial sitting load to decrease the risk of pressure ulcers. Arch Phys Med Rehabil 2007;88(7):862–70.
[10] Gefen A. The biomechanics of sitting-acquired pressure ulcers in patients with spinal cord injury or lesions. Int Wound J 2007;4(3):222–31.
[11] Gefen A. Reswick and Rogers pressure-time curve for pressure ulcer risk. Part 2. Nurs Stand 2009;23(46):40–4.
[12] Wu YK, Liu HY, Kelleher A, Pearlman J, Cooper RA. Evaluating the usability of a smartphone virtual seating coach application for powered wheelchair users. Med Eng Phys 2016;38(6):569–75.
[13] Liu HS, Cooper R, Kelleher A, Cooper RA. An interview study for developing a user guide for powered seating function usage. Disability Rehabil Assistive Technol 2014;9(6):499–512.
[14] Sonenblum SE, Vonk TE, Janssen TW, Sprigle SH. Effects of wheelchair cushions and pressure relief maneuvers on ischial interface pressure and blood flow in people with spinal cord injury. Arch Phys Med Rehabil 2014;95(7):1350–7.
[15] Liu HY, Grindle GG, Chuang FC, Kelleher A, Cooper R, Sieworek D, Smailigic A, Cooper RA. User preferences for indicator and feedback modalities: a preliminary survey study for developing a coaching system to facilitate wheelchair power seat function usage. IEEE Pervasive Comput Mobile Ubiquitous Syst 2012;11(3):54–63.
[16] Liu HY, Cooper RA, Cooper R, Smailagic A, Sieworek D, Ding D, Chuang FC. Seating virtual coach: a smart reminder for power seat function usage. Technol Disability 2010;22(1, 2):53–60.
[17] Ding D, Leister E, Cooper RA, Cooper R, Kelleher A. Usage and effectiveness of power wheelchair seating functions in the natural environment of wheelchair users. J Rehabil Res Dev 2008;47(7):973–84.
[18] Beeckman D, Defloor T, Schoonhoven L, Vanderwee K. Knowledge and attitudes of nurses on pressure ulcer prevention: a cross-sectional multicenter study in belgian hospitals. Worldviews Evid Based Nurs 2011;8(3):166–76.
[19] Stephens M, Bartley CA. Understanding the association between pressure ulcers and sitting in adults what does it mean for me and my carers? Seating guidelines for people, carers and health & social care professionals. J Tissue Viability 2018;27(1):59–73.
[20] McInnes E, Jammali-Blasi A, Bell-Syer S, Dumville J, Cullum N. Preventing pressure ulcers–Are pressure-redistributing support surfaces effective? A cochrane systematic review and meta-analysis. Int J Nurs Stud 2012;49(3):345–59.
[21] Levy A, Kopplin K, Gefen A. An air-cell-based cushion for pressure ulcer protection remarkably reduces tissue stresses in the seated buttocks with respect to foams: finite element studies. J Tissue Viability 2014;23(1):13–23.
[22] Wu GA, Bogie KM. Effects of conventional and alternating cushion weight-shifting in persons with spinal cord injury. J Rehabil Res Dev 2014;51(8):1265–76.
[23] Stockton L, Rithalia S. Is dynamic seating a modality worth considering in the prevention of pressure ulcers? J Tissue Viability 2007;17(1):15–21.
[24] Yu CH, Chou TY, Chen CH, Chen P, Wang FC. Development of a modularized seating system to actively manage interface pressure. Sensors (Basel) 2014;14(8):14235–52.
[25] Freeto T, Mitchell SJ, Bogie KM. Preliminary development of an advanced modular pressure relief cushion: testing and user evaluation. J Tissue Viability 2018;27(1):2–9.

[26] Nuthi P, Carrigan W, Pande C, Wijesundara MBJ. Control implementation for real-time pressure adjusting seat cushion to prevent pressure ulcers. In: Proceedings of the ASME 2018 international design engineering technical conferences & computers and information in engineering conference, DETC2018-86210, Quebec City, Quebec, Canada; 2018.
[27] Sonenblum SE, Sprigle SH, Cathcart JM, Winder RJ. 3D anatomy and deformation of the seated buttocks. J Tissue Viablility 2015;24(2):51–61.
[28] Hamanami K, Tokuhiro A, Inoue H. Finding the optimal setting of inflated air pressure for a multi-cell air cushion for wheelchair patients with spinal cord injury. Acta Med Okayama 2004;58(1):37–44.
[29] Cooper RA, Ohnabe H, Hobson DA. An introduction to rehabilitation engineering. Boca Raton, FL: Taylor and Francis Group LLC; 2006.
[30] Aissaoui R, Kauffmann C, Dansereau J, de Guise JA. Analysis of pressure distribution at the body-seat interface in able-bodied and paraplegic subjects using a deformable active contour algorithm. Med Eng Phys 2001;23(6):359–67.
[31] Baranoski S, Ayello E. Wound care essentials: practice principles. 4th ed. Philadelphia, PA: Lippincott Williams & Wilkins; 2015.
[32] Anderson S, Goede B, Kramer D, Leupp M, Nemunaitis G, Hefzy MS, Pourazady M. Correlating air cushion pressure to maximum interface pressure on the buttocks. In: Proceedings of the RESNA Annual Conference; 2013.
[33] Carrigan W, Nuthi P, Pande C, Wijesundara MBJ. A pressure modulating sensorized soft actuator array for pressure ulcer prevention. In: Proceedings of the ASME 2017 international design engineering technical conferences & computers and information in engineering conference, DETC2017-68191, Cleveland, Ohio, USA; 2017.
[34] Hollington J, Hillman SJ, Torres-Sánchez C, Boeckx J, Crossan N. ISO 16840-2:2007 load deflection and hysteresis measurements for a sample of wheelchair seating cushions. Med Eng Phys 2014;36(4):509–15.
[35] International Organization for Standardization. BS ISO 16840-2:2007 wheelchair seating—Part 2 determination of physical and mechanical characteristics of devices intended to manage tissue integrity—seat cushions. London: British Standards Institute; 2007.
[36] Horváth RM, Antal RM, Domljan D, Dénes L. Body pressure distribution maps used for sitting comfort visualization. Sigurnost 2017;59(2):123–32.